Journal of Applied Polymer Science

Shape-memory behaviors of electrospun chitosan/poly(ethylene oxide) composite nanofibrous membranes

Hongqiu Wei,[1] Fenghua Zhang,[1] Dawei Zhang,[2] Yanju Liu,[3] Jinsong Leng[1]

[1]Center for Composite Materials and Structures, Harbin Institute of Technology, Harbin 150080, People's Republic of China
[2]Department of Materials Science and Engineering, Northeast Forestry University, Harbin 150040, People's Republic of China
[3]Department of Astronautical Science and Mechanics, Harbin Institute of Technology, Harbin 150080, People's Republic of China
Correspondence to: J. Leng (E-mail: lengjs@hit.edu.cn)

ABSTRACT: With aim of constructing a class of functional environmentally friendly materials, we electrospun chitosan (CS) blends with various contents of poly(ethylene oxide) (PEO) into a series of composite nanofibrous membranes exhibiting shape-memory behaviors. In the present composite system, CS and PEO served as hard and soft domains, respectively. The CS, presenting no thermal transition, and the PEO, with apparent melting–crystallization, were demonstrated by differential scanning calorimetry testing. Characterizations also revealed that the morphologies of the CS/PEO membranes were controlled by the mass ratios of CS/PEO. The composite fibrous membranes showed great mechanical performances and thermal stabilities as well. Moreover, CS/PEO possessed excellent shape-memory behaviors. Such fibrous membranes could complete their shape-recovery processes within 20 s at the temperature of 20°C above the melting transition temperature (T_m). Both the shape fixity and shape-recovery ratios were higher than 90%, even after five cycles. The CS/PEO fibrous membranes present significant potential applications in the field of biotechnology and tissue engineering, such as in scaffolds and smart tubes. © 2015 Wiley Periodicals, Inc. J. Appl. Polym. Sci. **2015**, *132*, 42532.

KEYWORDS: biomaterials; composites; electrospinning; nanostructured polymers; stimuli-sensitive polymers

Received 15 April 2015; accepted 22 May 2015
DOI: 10.1002/app.42532

INTRODUCTION

Shape-memory polymers (SMPs) have been witnessed great developments in recent years. SMPs, a kind of stimulus-responsive polymers, feature a particular capability to revert to their initial shape from temporary shape exposure to heat,[1–3] solvents,[4] light,[5,6] electric and magnetic fields,[7,8] and different pH values.[9] Structurally, there are two important features, hard domains and soft domains, existing in SMPs. The combination of the two parts contributes to the shape-memory effect.[10] Hard domains, including chemically crosslinked points, molecular chain entanglements, and crystallization phases, function to record the permanent shape. Soft domains play key roles in switching the temporary shape; this may be a glassy/rubbery transition, crystal/melting transition, or reversible molecules crosslinks.[11,12] Such unique shape-memory behavior endows SMPs with various potential applications, ranging from deployable structures to biomedical devices.[10,13–16] So far, numerous studies on SMPs have been presented. With the recent developments of miniaturizing smart materials and devices, it is necessary to process SMPs with microstructures or nanostructures; this enables broader applications to meet smart, biomedical, and flexible functional needs.[17–20]

Electrospinning is an effective technology for manufacturing microfibrous or nanofibrous membranes.[21–27] It is well known that ultramicroscopic structures affect the properties of materials quite a great deal. Compared with blocks, electrospun microfibrous or nanofibrous membranes exhibit a plenty of advantages, including a large surface area, porous structure, high aspect ratio, and feasible processability.[28–35] Once the electrospinning method is applied to SMPs, an indication that microstructures or nanostructures have been given to them, smart performances of SMPs may be further facilitated or magnified. On the basis of these assumptions, electrospun shape-memory microfibrous or nanofibrous membranes have emerged in recent years, and a series of significant results have been obtained.[36–43] For example, Hu *et al.*[36,37] at Hong Kong Polytechnic University reported an electrospun fabric exhibiting a dual-shape-memory effect, which was fabricated from shape-memory polyurethane. Cao *et al.*[40] prepared a shape-memory nonwoven film with a stable fibrous structure via the

Table I. Viscosity Values of the Pure CS and CS/PEO Solutions

Sample	CS	C4P1	C4P2	C4P3	C4P4	C4P5
Viscosity (mPa s)	123.8	182.6	291.2	442.4	593.6	810.0

electrospinning of a triethoxysilane end-capped polyurethane solution and demonstrated that the recovery speed of such fibrous SMP films was faster than that of the block. Our group recently exhibited an interesting Nafion-based nanofibrous membrane possessing quintuple-shape-memory performances.[41]

Although electrospun SMPs have been demonstrated, the majority of which are synthesized in laboratory.[44–47] To develop sustainable and environmental friendly materials, natural materials are indispensable and crucial. Chitosan (CS), as a typical type of natural polymer derived from chitin deacetylation, possesses excellent biological functionality and compatibility, security, antimicrobial capability, and biodegradability.[48,49] During the past few years, CS-based fibrous membranes have been fabricated and applied in various fields, such as tissue engineering, drug release, and food packing.[50–54] However, CS-based fibrous membranes have seldom been developed as shape-memory materials. On the basis of abundant amine and hydroxyl groups in the molecular structure,[48] the melting temperature (T_m) of CS is always higher than the its decomposition temperature (T_d).[55] Therefore, CS shows great potential to act as hard segments in shape-memory networks. To construct CS with shape-memory behavior, in this study, poly(ethylene oxide) (PEO) with a notable crystal/melting transition was introduced to the CS network and used as soft segments via an electrospinning method. We systematically investigated the performances of the electrospun CS/PEO fibrous membranes, demonstrating that this polymeric system exhibited excellent nanofibrous morphology and thermal and mechanical properties. Furthermore, such CS/PEO composite nanofibrous membranes presented remarkable dual-shape-memory effect and a fast, responsive speed. With the superior functions and nanofibrous structures, electrospun CS/PEO shape-memory nanofibrous membranes (SMNMs) can broaden their applications in majority of areas, especially for smart materials and structures.

EXPERIMENTAL

Materials

CS was supplied by Zhejiang Golden-Shell Pharmaceutical Co., Ltd., with a 75–85% deacetylation degree. PEO (number-average molecular weight = 900,000) was obtained from Changchun Jinghua Co., Ltd. Acetic acid (analytical grade) was commercially available from Aladdin Industrial, Inc. Deionized water was used in this study. All of the materials were used as received without further treatment.

Electrospinning of the CS/PEO Nanofibers

A certain amount of CS was dissolved in acetic acid solution (2% v/v) via continuous magnetic stirring for 24 h to prepare a 2 wt % CS homogeneous solution. Appropriate amounts of PEO were added to the 2 wt % CS solution and stirred for another 12 h. Then, CS/PEO blend solutions with different mass ratios CS to PEO (4 : 1, 4 : 2, 4 : 3, 4 : 4, and 4 : 5, named C4P1, C4P2, C4P3, C4P4, and C4P5, respectively) were obtained. The viscosity values of the CS and CS/PEO solutions are listed in Table I; they were tested by a rotational viscometer with a speed of 100 rpm. All of the experimental procedures were undertaken at room temperature.

The CS/PEO SMNMs were prepared via a laboratory electrospinning instrument (Nanospider, Elmarco). The electrospinning of 30 mL of CS/PEO solution was conducted by the application of a high-voltage power of 45 kV, a 20-cm electrode-to-collector distance, and an electrode rotation rate of 0.9 rpm. An electronic conductible paper was used to collect the electrospun products. The whole process was undertaken at the ambient temperature of 25 ± 2°C for 1 h with a relative humidity of less than 45%. After electrospinning, the prepared membrane was dried at 35°C for 24 h in a vacuum oven. Finally, the sample was separated from the electronic conductible paper for characterizations. The schematic diagram of the electrospinning process and the macroscopic picture of the prepared CS/PEO nanofibrous membrane are shown in Figure 1(a,b), respectively. The average thickness of the obtained membranes was about 0.15 mm.

Characterization

The morphology and structure of the electrospun CS/PEO membranes were investigated by Scanning electron microscopy (SEM; Quanta 200FEG). All samples were gold-sputtered for 15 min before observation. The diameters of the nanofibers were measured with Image J software by the random choice of 100 fibers. The three-dimensional surface topologies were observed by laser confocal microscopy (LCM; OLS4100, Olympus) with noncontact mode.

The chemical composition of the CS/PEO nanofibrous films were analyzed by Fourier transform infrared (FTIR) spectroscopy (PE Spectrum One). The experiment was undertaken under a spectral range of 4000–650 cm^{-1} and a resolution of 4 cm^{-1}.

Thermogravimetric analysis (TGA; DSC1 SF1942, Mettler-Toledo) was conducted from 25 to 800°C at a heating rate of 10°C/min under nitrogen conditions.

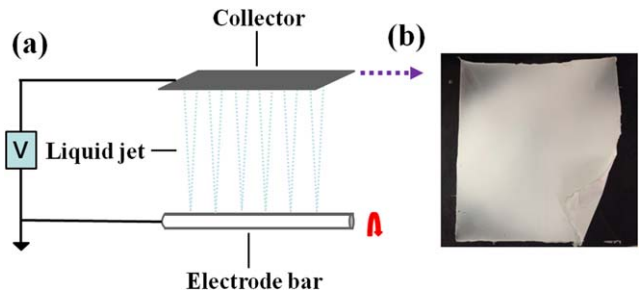

Figure 1. Schematic diagram of electrospinning process (a); macroscopic picture of prepared CS/PEO membrane (b). [Color figure can be viewed in the online issue, which is available at wileyonlinelibrary.com.]

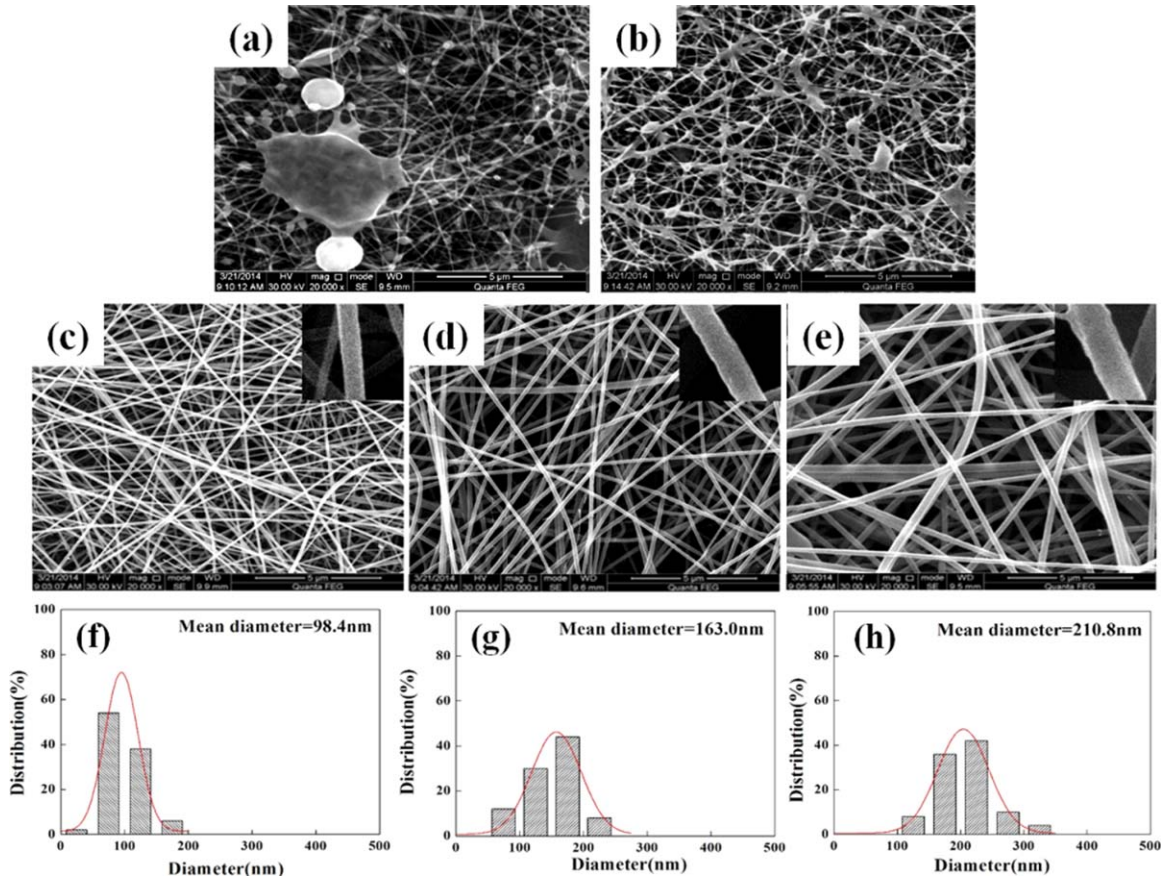

Figure 2. SEM images of the CS/PEO composite membranes at a magnification of 20,000×: (a) C4P1, (b) C4P2, (c) C4P3, (d) C4P4, and (e) C4P5. Histograms of the nanofiber diameter distribution of (f) C4P3, (g) C4P4, and (h) C4P5. [Color figure can be viewed in the online issue, which is available at wileyonlinelibrary.com.]

The thermal transition performances of the obtained CS/PEO membranes were observed with differential scanning calorimetry (DSC; 700/1410, Mettler-Toledo). The test was performed at temperatures ranging 25 to 200°C at a heating or cooling rate of 10°C/min in a nitrogen atmosphere. To eliminate the influences of the heat history, the cooling and secondary heating results were adopted for the final analysis.

The mechanical properties were carried out by a commercial nanotensile testing system (Nano UTMTM universal testing system T150, Agilent Technologies) according to the method UTM-Bionix Standard Toecomp CDA. The tensile strain rate was set as 0.1 mm/s.

The dual-shape-memory effect was examined by a bending-recovery experiment. The CS/PEO SMNMs were cut into rectangular strips with dimensions of 50 × 5 × 0.15 mm^3 as initial shapes. To obtain the temporary U shapes, the specimens were put into an oven at $T_m + 20$°C. After being preheated for 1 min, the samples were completely soft. Such heated samples

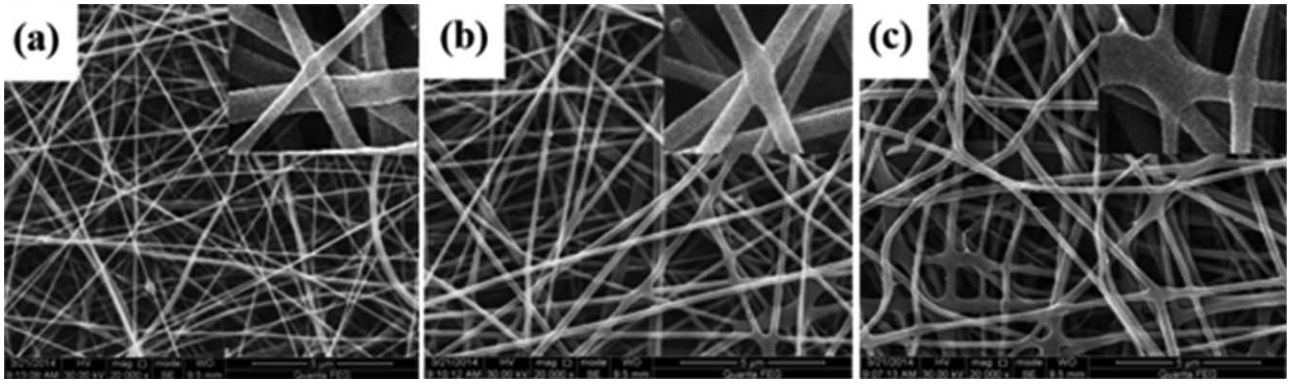

Figure 3. SEM images of CS/PEO composite membranes after drying at a magnification of 20,000×: (a) C4P3; (b) C4P4; (c) C4P5.

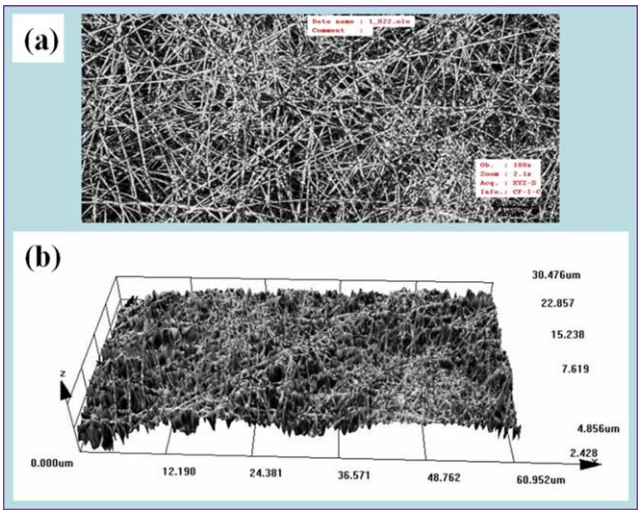

Figure 4. LCM results for the C4P4 membrane: (a) two-dimensional and (b) three-dimensional images of the surface topology. [Color figure can be viewed in the online issue, which is available at wileyonlinelibrary.com.]

were bent into U shapes around a corresponding shaped mold. The external force was retained until the temperature was cooled down to 25°C at a rate of 20°C/min. Then, the deformed U shapes were reserved upon the release of the external force. The U-shaped specimens were subsequently reheated to $T_m + 20$°C at a healing rate of 20°C/min. The expected occurrence of the shape-memory behavior was observed. The whole process was monitored by a video recorder. The shape fixity ratio (R_f), shape-recovery ratio (R_r), and shape-recovery time (T_r) were used to quantitatively analyze the shape-memory effect. R_f and R_r were determined as follows:[4,40]

$$R_f = \frac{180^\circ - \theta_f}{180^\circ} \quad (1)$$

$$R_r = \frac{\theta_r}{180^\circ} \quad (2)$$

where θ_f is the release angle after the removal of an external force at 25°C and θ_r is the recovery angle. T_r, θ_f, and θ_r were provided by the video recording.

RESULTS AND DISCUSSION

Morphologies of the Electrospun CS/PEO Composite Membranes

The CS/PEO SMNM composites were processed by electrospinning. The mass ratios of CS/PEO in the solution influenced the morphologies of the nanofibers. Figure 2 shows the SEM images of the morphologies of the electrospun CS/PEO membranes with different contents of PEO before drying. The primitive morphologies of these electrospinning products were obtained. It was clear that the structures of the CS/PEO SMNMs presented droplet or beaded forms at low PEO contents [Figure 2(a,b)]. As the PEO content increased, the morphology experienced a dramatic transformation. Bead-free continuous nanofibers were successfully produced when the mass ratios of CS to PEO increased from 4 : 3 to 4 : 5 [Figure 2(c–e)]. Furthermore, the addition of PEO influenced the mean diameters of these nanofibers, which changed from 98.4 to 210.8 nm [Figure 2(h,g)].

The reasons contributing to the previous results were expounded in a previous study.[53,56–59] Briefly, CS is a typical kind of ionic polymers. In a 2% v/v acetic acid solution (acidic condition), the ionic functional groups (—NH_2 and —OH) belonging to CS had the ability to be ionized; this resulted in the appearance of a charge. For the solution with a high CS concentration (C4P1 and C4P2), the applied high voltage caused a relatively high charge density on the surface of the polymer-jet generated from the collector; this indicated that a huge repulsive force existed in the ionic groups. We considered that the enormous repulsion constructed the polymer jet to droplet and beaded forms. When the contents of the nonionic polymer PEO increased, the concentration of the ionic polymer CS decreased. This suggested that the reduction of the repulsive force was beneficial for the formation of smooth fibers (C4P3). However, overintroduction of the nonionic polymer PEO was not suitable for producing fibers with small diameters. PEO at a high concentration reduced the charge density inside the solution. In other words, the charge–charge repulsion that reacted on the opposite direction of the surface tension decreased; this manifested that the formation of small-diameter fibers was affected. Thus, the CS/PEO mass ratio could be treated as one of the crucial elements in controlling the morphology and diameter of the electrospun nanofibers. Because of the noncontinuous fibrous structures of C4P1 and C4P2, the following characterizations are mainly focused on the samples C4P3, C4P4, and C4P5.

Figure 3 presents SEM images of the CS/PEO nanofibrous membranes after drying. It is clear that the morphologies of the C4P3, C4P4, and C4P5 composite membranes still showed stable nanofibrous networks after the drying process. Only a few changes, such as shrink and deformation, were observed. The reasons for the variations of the nanofibers can be summarized by two aspects. One was the disappearance of the residual solvent and stress during the drying process. The other one was that the drying procedure may have gradually led to the occurrence of a melting transition behavior in PEO.

LCM was carried out to further investigate the morphologies of the CS/PEO SMNMs, and C4P4 was used as an example. Figure 4

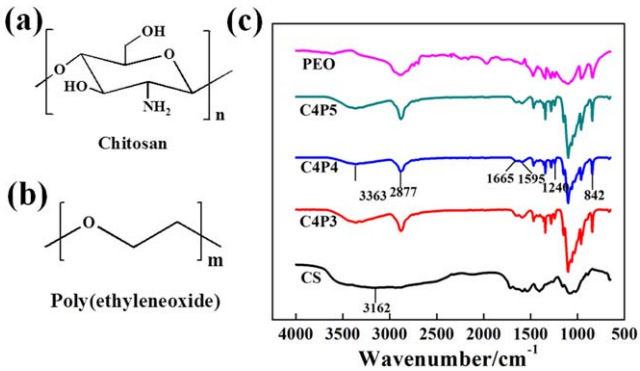

Figure 5. Molecule of CS (a) and PEO (b); FT-IR spectrums of CS/PEO SMNMs (c). [Color figure can be viewed in the online issue, which is available at wileyonlinelibrary.com.]

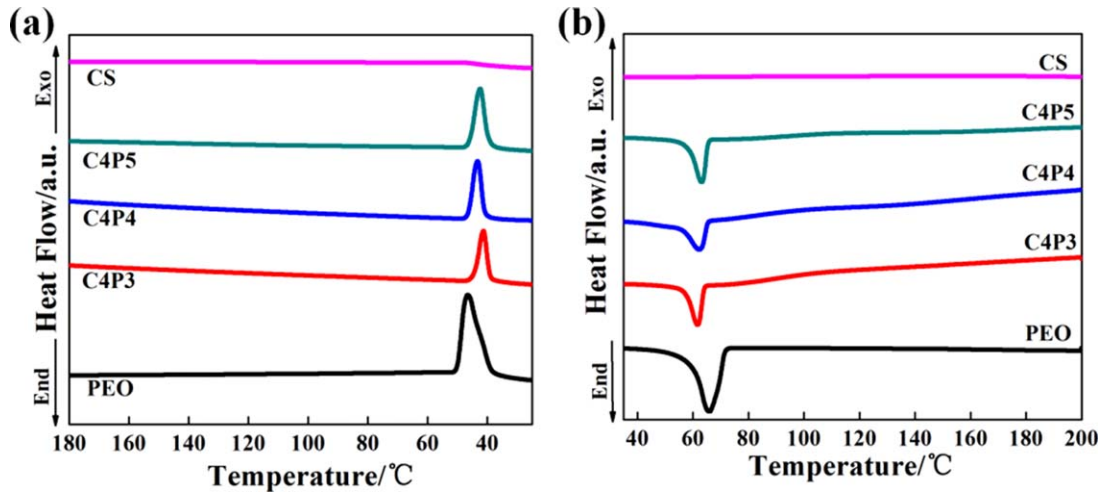

Figure 6. DSC curves of the (a) cooling scans and (b) second heating scans for the pure CS, pure PEO, and CS/PEO SMNMs. [Color figure can be viewed in the online issue, which is available at wileyonlinelibrary.com.]

shows the LCM results of C4P4. The two-dimensional image of the C4P4 surface [Figure 4(a)] presents continuous nanofibers; this was in accordance with the SEM pictures. From three-dimensional surface topology [Figure 4(d)], the surface of C4P4 was relatively neat; this indicated that the nanofibers deposited uniformly. The LCM images also demonstrated that the fibrous nonwoven membrane was successfully produced.

Chemical Structures of the CS/PEO SMNMs

Figure 5 presents the molecular structures of CS and PEO and the FTIR spectra of the CS/PEO SMNMs at 4000 to 650 cm^{-1}. As shown in Figure 4(c), the CS/PEO composite membranes exhibited absorption peaks at 1665 and 1595 cm^{-1}, which corresponded to amide I and amide II, respectively, and belonged to CS.[51,53] The absorption peaks at 1240 and 842 cm^{-1} were assigned to PEO.[60,61] The obtained results could also be verified by the molecular structures of CS and PEO, as shown in Figure 4(a,b). The peak at 2877 cm^{-1} was ascribed to the stretching vibrations of —CH_2— bonds and became more visible. Also, the wide band at about 3162 cm^{-1} stood for the stretching vibrations of O—H, and the N—H band moved to 3363 cm^{-1} and become narrow, compared with that of CS. These changes were attributed to the increase in the PEO content. In addition, no other peaks emerged or disappeared, except for the characteristic peaks of CS and PEO. These results demonstrate that both CS and PEO were successfully electrospun in the membranes without chemical reaction.

Thermal Properties of the CS/PEO SMNMs

A DSC experiment as one type of thermoanalysis technology was used to investigate the phase-transition behavior of the pure CS, CS/PEO SMNMs, and pure PEO. The cooling and second heating curves are shown in Figure 6. Some parameters, including T_m, enthalpy of fusion (ΔH_m), and crystallization temperature (T_c), are listed in Table II. For pure PEO, a strong endothermic peak was perceived at 65.84°C (T_m) in the heating trace; this was ascribed to the melting transition of PEO. Accordingly, in the cooling cycle, an apparent exothermic peak emerged at 46.45°C (T_c); this corresponded to the crystallization behavior of PEO. The phase-transition performance of pure CS is always a disputable subject. Some studies have reported that the glass-transition behavior was monitored to be around 203°C.[62] However, other studies have demonstrated that CS showed a glass-transition temperature at a higher temperature where thermal decomposition prevented its occurrence.[55] Such dramatic differences were attributed to the different resources and extractive and fabricated methods.[63] In this study, both the heating and cooling DSC scans of CS were approximately straight lines; this indicated that CS had no obvious phase transition from 35 to 200°C. With increasing PEO content, T_m and T_c values of CS/PEO SMNMs present rising trends. This

Table II. Thermal Properties of the Pure CS, PEO, and CS/PEO SMNMs

	DSC				TGA	
Sample	T_m (°C)	ΔH_m (J/g)	T_c (°C)	T_d (°C)	T_{max} (°C)	Char yield (%)
CS	—	—		171	185, 275	31
C4P3	61.28	7.73	41.40	268	126.9, 286.4, 412.3	17
C4P4	62.29	8.81	42.71	272	125.8, 283.5, 409.1	15
C4P5	63.68	10.79	43.51	282	124.9, 282.9, 408.5	13
PEO	65.84	24.21	46.45	380	403.5	8

T_d, decomposition temperature at which 5% loss of weight is observed. The T_{max} was related to each peak in DTG curves.

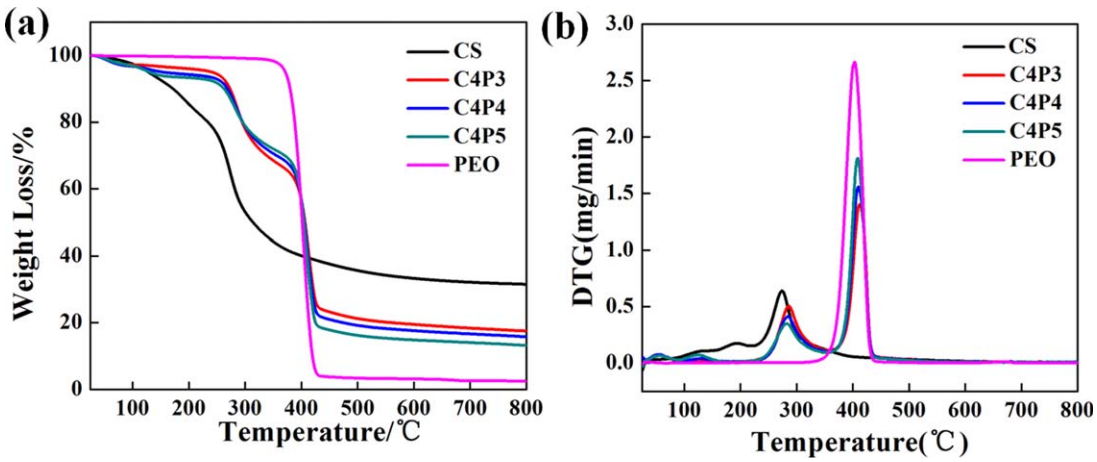

Figure 7. (a) TG and (b) DTG curves of the CS/PEO SMNMs. [Color figure can be viewed in the online issue, which is available at wileyonlinelibrary.com.]

indicated that the crystallinities of CS/PEO SMNMs increased gradually. Such variation was attributed to the fact that the increasing PEO content resulted in stronger molecular interactions. More importantly, both T_m and T_c of CS/PEO SMNMs quite approached to the values of pure PEO. There was no trace of the thermal transition of CS. The previous results manifest that the thermal transitions of the CS/PEO SMNMs were mainly due to the melting–crystallization transition of PEO. It is the design principle for the shape-memory effect. CS possessing no phase transition is constructed to the hard domains for memorizing the permanent shapes of membranes. PEO, along with its melting–crystallization, is the soft domains, which were responsible for temporary shapes.

The thermal stabilities of the CS, PEO, and CS/PEO SMNMs series were investigated by TGA in a nitrogen atmosphere at temperatures ranging from 25 to 800°C. The experimental results are given in Figure 7. Some elements of the curves, including two particular temperatures, T_d and T_{max} (defined as the temperature of each peak in DTG curves), the thermal degradative stage, and the char yield, were deeply examined and are shown in Table II. In the thermogravimetry (TG) curves [Figure 7(a)], only one thermal degradative stage of pure PEO was observed; this began at 380°C (T_d) and was accomplished at about 446°C with an 8% char residual value. T_d of pure CS was 171°C, and the two thermal degradative stages were as follows. The first one appeared from 171 to 246°C and corresponded to the weight loss from 10 to 24%. This was due to the vaporization and decomposition of residual acetic acid molecules. The second evident stage was monitored between 246 and 400°C, where the majority of weight loss occurred; this indicated the decomposition of CS network. A char yield of CS was 31% at the end. The previous results were in accordance with previous studies.[56] The T_d values of C4P3, C4P4, and C4P5 started at 268, 272, and 282°C, respectively. The subsequent performances showed three steps, which corresponded to the decomposition of residual acetic acid molecules, the CS network, and the PEO backbone, respectively. Further observation showed that the residual char values of the three samples were 17, 15, and 13%. The T_{max} related to each peak in the DTG curves is shown in Figure 5(b). Obviously, T_{max} of PEO is 403.5°C. The pure CS possessed two T_{max} values in the DTG curve at 185 and 275°C, respectively. For the CS/PEO SMNMs, T_{max} presented three peaks, which were around 125, 286, and 412°C, respectively.

From the previous results, it was apparent that the thermal degradative behavior of the CS/PEO SMNMs exhibited thermal decomposition characteristics of both PEO and CS; this suggested the presence of CS and PEO in the SMNMs without chemical reaction and supported the consequences of the FTIR experiment. Furthermore, for the CS/PEO SMNMs, there was

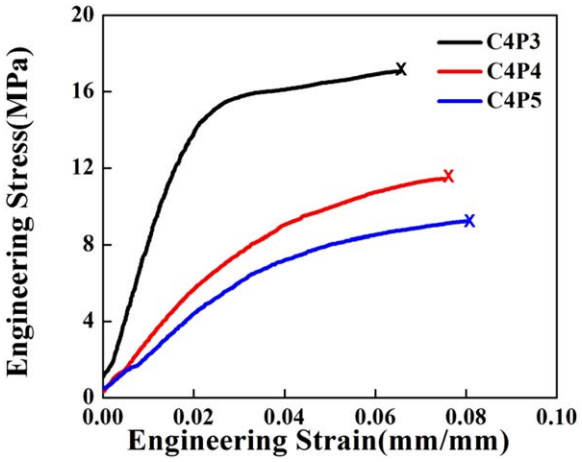

Figure 8. Engineering strain–stress curves of the CS/PEO SMNMs. [Color figure can be viewed in the online issue, which is available at wileyonlinelibrary.com.]

Table III. Typical Mechanical Parameters of the CS/PEO SMNMs Obtained from Nanotensile Testing

Sample	E (MPa)	σ_b (MPa)	ε_b (%)
C4P3	548.05 ± 11.44	18.25 ± 1.89	0.069 ± 0.0058
C4P4	274.17 ± 8.13	12.36 ± 1.53	0.075 ± 0.0036
C4P5	242.76 ± 13.91	10.27 ± 1.83	0.087 ± 0.0048

Table IV. R_f, R_r, and T_r of the First Three Shape-Recovery Processes of the CS/PEO SMNMs

Sample	Shape-memory results	First	Second	Third	Average
C4P3	R_f (%)	96.67	95.56	97.22	96.48
	R_r (%)	90.00	92.22	91.11	91.11
	T_r (s)	18	16	21	18.33
C4P4	R_f (%)	95.00	94.44	92.78	94.07
	R_r (%)	95.56	95.00	93.89	94.82
	T_r (s)	19	14	15	16
C4P5	R_f (%)	91.67	89.44	90.56	90.56
	R_r (%)	94.44	96.11	95.00	95.18
	T_r (s)	12	15	20	15.67

no dramatic variations in T_d, T_{max}, and residual char yield. This illustrated that different PEO contents slightly influenced the thermal behavior of the CS/PEO SMNMs.

Mechanical Properties of the CS/PEO SMNMs

The mechanical properties of the SMNMs were characterized by a nanotensile testing system. The tensile stress–strain curves of C4P3, C4P4, and C4P5 are shown in Figure 8. Some mechanical parameters, such as the Young's modulus (E), maximum tensile strength (σ_b), and elongation at break (ε_b), were obtained and are summarized in Table III. The CS/PEO SMNMs showed a high E and σ_b together with a low ε_b. The relatively brittle mechanical behavior was mainly attributed to the high crystallinity of CS.[53] With increasing PEO content, E decreased from 548.05 ± 11.44 to 242.76 ± 13.91 MPa, and σ_b changed from 18.25 ± 1.89 to 10.27 ± 1.83 MPa. Oppositely, ε_b presented an apparent rising trend ranging from 0.069 ± 0.0058 to 0.087 ± 0.0048 MPa. Such changes indicated that the toughness of the CS/PEO SMNMs increased to some degree with the introduction of PEO because of its flexible linear aliphatic segments.

Shape-Memory Performances of the CS/PEO SMNMs

The shape-memory behaviors of the CS/PEO SMNMs were examined by the bending-recovery test. The deformation temperature and recovery temperature of C4P3, C4P4, and C4P5 were set at $T_m + 20$°C. Table IV presents the shape-memory results of the first three shape-memory circles of C4P3, C4P4, and C4P5, including R_f, R_r, and T_r. With increasing PEO content, the average R_f and T_r decreased, and the average R_r exhibited a rising trend. The results indicate that the increase in PEO provided superior shape-recovery properties, whereas the shape fixity performances decreased somewhat. The increasing reversible phase PEO indicated more active molecule segments, which endowed the material with far better deformability and recovery capacity. However, an excess of PEO led to a less fixed-phase CS and led to a worse shape fixity. From further observation, We found that the average R_f and R_r of C4P3, C4P4, and C4P5 were higher than 90%. The highest R_f and R_r were up to 97.22 and 96.11%, respectively. The average T_r of the three compositions was less than 20 s, and the shortest one was just 12 s. The experimental data demonstrated that the CS/PEO SMNMs

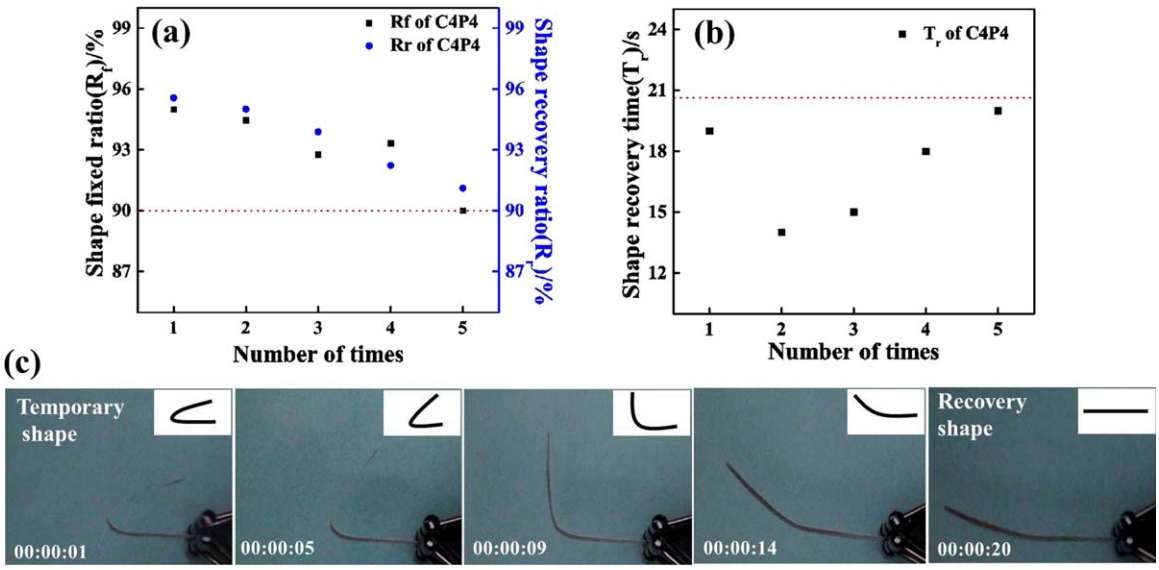

Figure 9. Shape-memory behavior of the five shape-recovery processes of C4P4: (a) R_f and R_r, (b) T_r, and (c) visual demonstration of the fifth shape-recovery process of C4P4. [Color figure can be viewed in the online issue, which is available at wileyonlinelibrary.com.]

completed the shape-recovery process in a short period of time with a high R_f and R_r; this indicated that such fibrous membranes possessed an excellent shape-memory effect.

C4P4 was chosen for investigating for five shape-memory cycles on the basis of its less average T_r and relatively high and close average R_f and R_r. The shape-memory properties of C4P4 are presented in Figure 8. Figure 9(a) shows that each R_f and R_r were greater than 90%. The averages were 93.11 and 93.56%, respectively. The whole T_r in Figure 9(b) was less than 20 s, and the average was merely 17.2 s. The results indicate that C4P4 demonstrated excellent and repeatable shape-memory performances. Figure 9(c) presents the visual demonstration of the fifth shape-recovery process of C4P4. Clearly, the sample could recover its original strip shape from the temporary U shape with a fast, responsive speed.

CONCLUSIONS

In summary, a series of nanofibrous membranes with shape-memory properties were constructed successfully on the basis of CS and PEO via electrospinning technology. In this shape-memory composite system, CS exhibiting no thermal transition was used as the hard domain to memorize the permanent shape, and PEO was used as the soft domain to complete the deformed or recovery process on the basis of its melting–crystallization. The mass ratio of CS/PEO had a significant influence on the morphologies of these SMNMs. Smooth fibers began to form at a mass ratio of 4:3. Such materials presented great thermal stability. Moreover, such CS/PEO fibrous membranes possessed excellent shape-memory behaviors. R_f and R_r were higher than 90%. T_r was less than 20 s. Along with the unique shape-memory effect, the CS/PEO nanofibrous membranes are expected to realize practical applications in the areas of smart materials and structures.

ACKNOWLEDGMENTS

This work was supported by the National Natural Science Foundation of China (contract grant numbers 11225211 and 11272106), and the authors are very grateful.

REFERENCES

1. Yang, C. S.; Wu, H. C.; Sun, J. S.; Hsiao, H. M.; Wang, T. W. *ACS Appl. Mater. Interfaces* **2013**, *5*, 10985.
2. Michal, B. T.; Jaye, T. A.; Spencer, E. J.; Rowan, S. *J. ACS Macro Lett.* **2013**, *2*, 694.
3. Xie, T.; Rousseau, I. A. *Polymer* **2009**, *8*, 1852.
4. Leng, J. S.; Lv, H. B.; Liu, Y. J.; Du, S. Y. *Adv. Eng. Mater.* **2008**, *10*, 592.
5. Lendlein, A.; Jiang, H. Y.; Junger, O.; Langer, R. *Nature* **2005**, *434*, 879.
6. Wu, Y.; Hu, J.; Zhang, C.; Han, J.; Wang, Y.; Kumara, B. *J. Mater. Chem. A* **2015**, *3*, 97.
7. Liu, Y. J.; Lv, H. B.; Lan, X.; Leng, J. S.; Du, S. Y. *Compos. Sci. Technol.* **2009**, *69*, 2064.
8. Razzaq, M. Y.; Behl, M.; Kratz, K.; Lendlein, A. *Adv. Mater.* **2013**, *25*, 5730.
9. Guo, W. W.; Lu, C. H.; Orbach, R.; Wang, F.; Qi, X. J.; Cecconello, A.; Seliktar, D.; Willner, I. *Adv. Mater.* **2015**, *27*, 73.
10. Leng, J. S.; Lan, X.; Liu, Y. J.; Du, S. Y. *Prog. Mater. Sci.* **2011**, *56*, 1077.
11. Meng, H.; Li, G. Q. *Polymer* **2013**, *54*, 2199.
12. Liu, C.; Qin, H.; Mather, P. T. *J. Mater. Chem.* **2007**, *17*, 1543.
13. Hu, J. L.; Zhu, Y.; Huang, H. H.; Lu, J. *Prog. Mater. Sci.* **2012**, *37*, 1720.
14. Lan, X.; Liu, Y. J.; Lv, H. B.; Wang, X. H.; Leng, J. S.; Du, S. Y. *Smart Mater. Struct.* **2009**, *18*, 024002.
15. Zhang, C. H.; Wei, H. G.; Liu, Y. Y.; Tan, H. F.; Guo, Z. H. *High Perform. Polym.* **2012**, *4*, 702.
16. Lendlein, A.; Langer, R. *Science* **2002**, *296*, 1673.
17. Zhang, P. F.; Li, G. Q. *J. Polym. Sci. Part B: Polym. Phys.* **2013**, *51*, 966.
18. Rana, S.; Kim, S. D.; Cho, J. W. *Polym. Adv. Technol.* **2013**, *24*, 609.
19. Peng, H. S.; Zhou, S. B.; Jiang, J.; Guo, T.; Zheng, X. T. *J. Phys. Chem. B* **2009**, *113*, 4636.
20. Tseng, L. F.; Mather, P. T.; Henderson, J. H. Bioengineering Conference (NEBEC), 2012 38th Annual Northeast, 16–18 March **2012**, 227.
21. Greiner, A.; Wendorff, J. H. *Angew. Chem. Int. Ed.* **2007**, *46*, 5670.
22. Zhu, J. H.; Wei, S. Y.; Patil, R.; Rutman, D.; Kucknoor, A. S.; Wang, A.; Guo, Z. H. *Polymer* **2011**, *52*, 1954.
23. Chen, X. L.; Wei, S. Y.; Gunesoglu, C.; Zhu, J. H.; Southworth, C. S.; Sun, L. Y.; Karki, A. B.; Young, D. P.; Guo, Z. H. *Macromol. Chem. Phys.* **2010**, *211*, 1775.
24. Liu, J.; Huang, J. N.; Wujcik, E. K.; Qiu, B.; Rutman, D.; Zhang, X.; Salazard, Wei, S. Y.; Guo, Z. H. *Macromol. Mater. Eng.* **2015**, *300*, 358.
25. Zhu, J.; Chen, M.; Qu, H.; Wei, H.; Luo, Z.; Haldolaarachchige, N.; Young, D. P.; Wei, S.; Guo, Z. H. *J. Mater. Chem. C* **2014**, *2*, 715.
26. Atabey, E.; Wei, S. Y.; Zhang, X.; Gu, H. B.; Yan, X. R.; Huang, Y. D.; Shao, L.; He, Q. L.; Zhu, J. H.; Sun, L. Y.; Kucknoor, A. S.; Wang, A.; Guo, Z. H. *J. Compos. Mater.* **2013**, *47*, 3175.
27. Zhu, J. H.; Wei, S. Y.; Zhang, L.; Mao, Y. B.; Ryu, J.; Haldolaarachchige, N.; Young, D. P.; Guo, Z. H. *J. Phys. Chem. C* **2010**, *114*, 8844.
28. Li, D.; Xia, Y. N. *Adv. Mater.* **2004**, *14*, 1151.
29. Zhu, J. H.; Wei, S. Y.; Rutman, D.; Haldolaarachchige, N.; Young, D. P.; Guo, Z. H. *Polymer* **2011**, *52*, 2947.
30. Chen, M. J.; Qu, H. L.; Zhu, J. H.; Luo, Z. P.; Khasanov, A.; Kucknoor, A. S.; Haldolaarachchige, N.; Young, D. P.; Wei, S. Y.; Guo, Z. H. *Polymer* **2012**, *53*, 4501.
31. Subbiah, T.; Bhat, G. S.; Tock, R. W.; Parameswaran, S.; Ramkumar, S. *J. Appl. Polym. Sci.* **2005**, *96*, 557.

32. Sharma, J.; Zhang, X.; Sarker, T.; Yan, X. G.; Washburn, L.; Qu, H. L.; Guo, Z. H.; Kucknoor, A.; Wei, S. Y. *Polymer* **2014**, *55*, 3261.
33. Huang, Z. M.; Zhang, Y. Z.; Kotaki, M.; Ramakrishna, S. *Compos. Sci. Technol.* **2003**, *15*, 2223.
34. Qu, H. L.; Wei, S. Y.; Guo, Z. H. *J. Mater. Chem. A* **2013**, *1*, 11513.
35. Zhang, D.; Karki, A. B.; Rutman, D.; Young, D. P.; Wang, A.; Cocke, D.; Ho, T. H.; Guo, Z. H. *Polymer* **2009**, *50*, 4189.
36. Zhuo, H. T.; Hu, J. L.; Chen, S. *J. Mater. Lett.* **2008**, *62*, 2074.
37. Zhuo, H. T.; Hu, J. L.; Chen, S. *J. Express Polym. Lett.* **2011**, *5*, 182.
38. Bao, M.; Lou, X. X.; Zhou, Q. H.; Dong, W.; Yuan, H. H.; Zhang, Y. *ACS Appl. Mater. Interfaces* **2014**, *6*, 2611.
39. Tseng, L. F.; Mather, P. T.; Henderson, J. H. *Acta Biomed.* **2013**, *9*, 8790.
40. Chen, H. L.; Cao, X. Y.; Zhang, J. N.; Zhang, J. J.; Ma, Y. M.; Shi, G. Q.; Ke, Y. C.; Tong, D. W.; Jiang, L. *J. Mater. Chem.* **2012**, *22*, 22387.
41. Zhang, F. H.; Zhang, Z. C.; Liu, Y. J.; Lv, H. B.; Leng, J. S. *Smart Mater. Struct.* **2013**, *22*, 085020.
42. Schneider, T.; Kohl, B.; Sauter, T.; Kratz, K.; Lendlein, A. *Clin. Hemorheol. Microcirc.* **2012**, *52*, 325.
43. Torbati, A. H.; Mather, P. T.; Reeder, J. E. *J. Biomed. Mater. Res. A* **2014**, *102*, 1236.
44. Fu, G. D.; Xu, L. Q.; Yao, F.; Li, G. L.; Kang, E. T. *ACS Appl. Mater. Interfaces* **2009**, *1*, 2424.
45. Dallmeyer, I.; Chowdhury, S.; Kadla, J. F. *Biomacromolecules* **2013**, *14*, 2354.
46. Ahn, J. S.; Yu, W. R.; Youk, J. H.; Ryu, H. Y. *Smart Mater. Struct.* **2011**, *20*, 105024.
47. Ko, Y. I.; Kim, B. S.; Bae, J. S.; Kim, Y. A.; Kim, I. S. *RSC Adv.* **2013**, *3*, 20091.
48. Chung, Y. C.; Yang, K.; Cho, J. W.; Chun, B. C. *Color. Technol.* **2014**, *130*, 305.
49. Rinaudo, M. *Prog. Polym. Sci.* **2006**, *7*, 603.
50. Kong, M.; Chen, X. G.; Xing, K.; Park, H. *J. Int. J. Food Microbiol.* **2010**, *144*, 51.
51. Li, W.; Luo, T.; Shi, Y.; Yang, Y. J.; Huang, X. S.; Xing, K. X.; Liu, L. F.; Wang, M. Q. *Integr. Ferroelectr.* **2014**, *151*, 164.
52. Chen, S.; Hao, Y. T.; Cui, W. G.; Chang, J.; Zhou, Y. *J. Mater. Sci.* **2013**, *48*, 6567.
53. Bonilla, J.; Fortunati, E.; Atarés, L.; Chiralt, A.; Kenny, J. M. *Food Hydrocolloids* **2014**, *35*, 463.
54. Shao, L.; Chang, X. J.; Zhang, Y. L.; Huang, Y. F.; Yao, Y. H.; Guo, Z. H. *Appl. Surf. Sci.* **2013**, *280*, 989.
55. Dhandayuthapani, B.; Krishnan, U. M.; Sethuraman, S. *J. Biomed. Mater. Res. B* **2010**, *1*, 264.
56. Tripathi, S.; Mehrotra, G. K.; Dutta, P. K. *Int. J. Biol. Macromol.* **2009**, *45*, 372.
57. Gautam, S.; Chou, C. F.; Dinda, A. K.; Potdar, P. D.; Mishra, N. C. *J. Mater. Sci.* **2014**, *49*, 1076.
58. Park, W. H.; Jeong, L.; Yoo, D. I.; Hudson, S. *Polymer* **2004**, *45*, 7151.
59. Zhang, Y.; Ouyang, H.; Lim, C. T.; Ramakrishna, S.; Huang, Z. M. *J. Biomed. Mater. Res. B* **2005**, *72*, 156.
60. Son, W. K.; Youk, J. H.; Lee, T. S.; Park, W. H. *Polymer* **2004**, *45*, 2959.
61. Cai, M. T.; Zhang, J. X.; Chen, Y. W.; Cao, J.; Leng, M. T.; Hu, S. D.; Luo, X. L. *Chin. J. Polym. Sci.* **2014**, *2*, 236.
62. Sakurai, K.; Maegawa, T. T.; Takahashi, T. *Polymer* **2000**, *41*, 7051.
63. Pereira, M. R. *Carbohydr. Polym.* **2005**, *62*, 97.